FINITE DIFFERENCE MODELING OF T-PHASE PROPAGATION FROM OCEAN TO LAND

Jeffry L. Stevens, G. Eli Baker, Heming Xu
Maxwell Technologies, Systems Division

Gerald D'Spain and Lewis P. Berger
Marine Physical Laboratory, Scripps Institution of Oceanography

Sponsored by U. S. Department of Defense
Defense Threat Reduction Agency
Contract No. DSWA01-97-C-0166

ABSTRACT

We model the T-Phase transition from ocean to land and evolution of the seismic signal through this process. We model the transition with a composite technique using normal mode based numerical propagation codes to calculate the hydroacoustic pressure field in the ocean, and use this pressure field as input for the elastic finite difference code TRES to calculate the seismic propagation to land-based stations. Animations are created from the finite difference calculations to help visualize the complex conversion process. We have performed a detailed study of the transition from the Point Sur interim IMS station to seismic stations along the California coast. The numerical calculations performed to date are accurate to 9 Hz.

An unusual result of the analysis that is observed both in the data and the calculations is that converted surface waves arrive at coastal stations earlier than body waves. This occurs because conversion to surface waves occurs farther offshore than conversion to body waves. For a typical coastal structure, the P-waves arrive in the middle of the surface wavetrain and are obscured at stations near the coast. T-phases propagate primarily as P-waves once they are well inland from the coast and the surface waves have been attenuated.

We have performed a number of test cases to assess the robustness of these results. Calculations for slopes varying from 10 degrees to 30 degrees show little difference in the results. Other studies have reported stronger effects for steeper slopes. All of the IMS T-Phase stations, however, are located in areas where the offshore slope is less than 30 degrees. The California calculations have a low velocity surface layer, so we performed a set of calculations with the ocean embedded in a uniform structure. Again, the results are similar with coastal waveforms dominated by surface waves. In a faster, more uniform structure, however, the P-wave may appear ahead of the surface wave for slopes of 30 degrees or higher.

We are continuing this research by performing calculations for paths to the IMS T-Phase stations, using the bathymetry along selected paths to those stations.

OBJECTIVE

The objective of this project is to better understand the propagation of T-phases from ocean to land, and the performance of T-phase International Monitoring System (IMS) stations, through empirical and numerical methods. The empirical study uses data from pressure sensors in the ocean and coastal and island seismometers to examine the T-phase transfer function. The numerical study uses finite difference calculations to model propagation of T-phases from ocean to land.

RESEARCH ACCOMPLISHED

The International Monitoring System (IMS) hydroacoustic network is a relatively sparse network consisting of 6 underwater hydroacoustic stations and 5 land-based seismic T-phase stations as shown in Figure 1. The hydroacoustic stations are much more sensitive to underwater signals than the T-phase stations and have a higher sampling rate and broader frequency range. The broader frequency range is important for identifying explosions, which are characterized by higher frequency content than other sources. Because of these limitations of T-phase stations, it is important to understand the efficiency of T-phase conversion in order to assess the capabilities of the IMS network for detection and identification of underwater sources. We are in the third year of a three year project to investigate these issues. In our presentations over the past two years, we described the following research:

1. Empirical estimates of T-phase transfer functions using T-phases from earthquakes at Hawaii/Loihi recorded on the Point Sur hydroacoustic station and seismometers in the UC Berkeley and PG&E networks.
2. Numerical modeling of these T-phases, and analysis of the waveforms. A movie of one of the calculations is available on the Internet at http://www.maxwell.com/products/geop/Movies/hydro.htm .

Our earlier papers (Stevens et al., 1998; Stevens et al., 1999) also described research into H-phases from small explosions off the California coast observed at IMS stations, research into far inland T-phases observed at distances as great as 1000 km from the coast, and research into modal decomposition of T-phases. This work is also described in two papers to be published in the special CTBT volume of Pure and Applied Geophysics (Stevens, et al, 2000; D'Spain et al, 2000). In addition, we have performed work under this contract on analysis of a large Russian hydroacoustic data set which we used to analyze the coupling of shallow explosion sources. This work has been presented at last year's symposium (Eneva et al, 1999) and in a third paper in the Pure and Applied Geophysics special issue (Eneva et al, 2000a) The most recent results are described in a paper in this symposium (Eneva et al, 2000b).

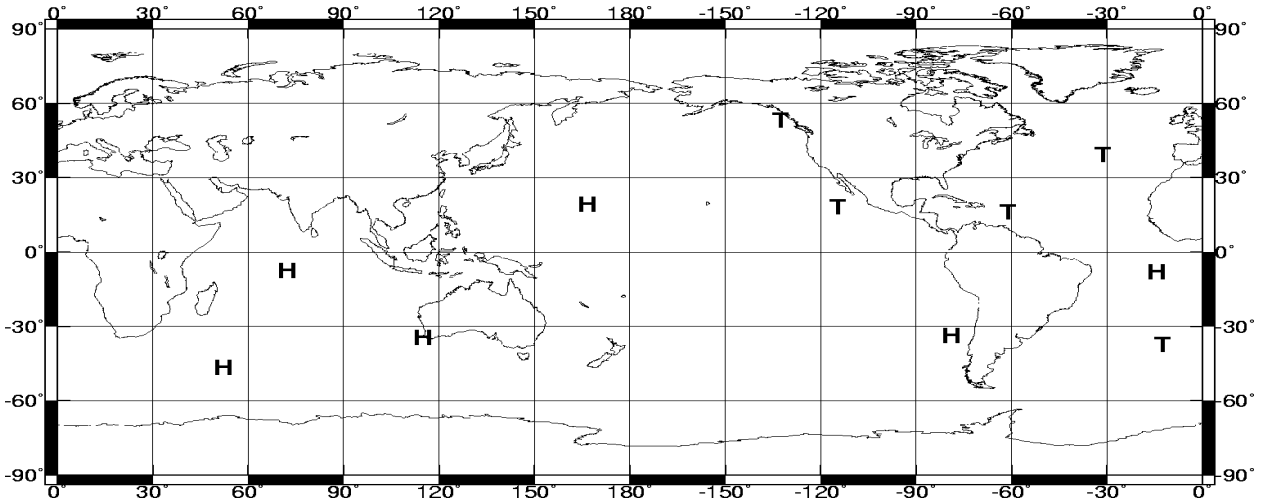

Figure 1. Hydroacoustic (H) and T-phase (T) stations in the future IMS network.

In the third year of this contract, most of the work on T-phase transfer functions has been directed towards extending the calculations to higher frequencies (from 4 Hz to 9 Hz), assessing the sensitivity of the results to a variety of physical parameters, and evaluating the implications of the results for IMS T-phase stations. In this paper, we first present a summary of the earlier work on T-phase transfer functions described in points 1 and 2 above, and then present the results of more recent work.

Observations of T-phase Transmission from the Ocean onto Land

We gathered data sets from events that were recorded on both underwater and coastal seismic stations for the purpose of directly measuring T-phase conversion. Four earthquakes from the emerging seamount Loihi and on the island of Hawaii generated very strong T-phases that impacted the California coast. We collected recordings of these events from the Point Sur (PSUR) hydroacoustic station, the Pacific Gas and Electric Central Coast seismic network (PG&E), and the Berkeley broadband digital seismic network (BDSN). The location of these stations and the bathymetry of the California continental shelf are shown in Figure 2. This is a nearly optimal situation for study of T-phase conversion because the hydroacoustic waves impact the coastline almost perpendicular to the coast as shown by the ray path on Figure 2.

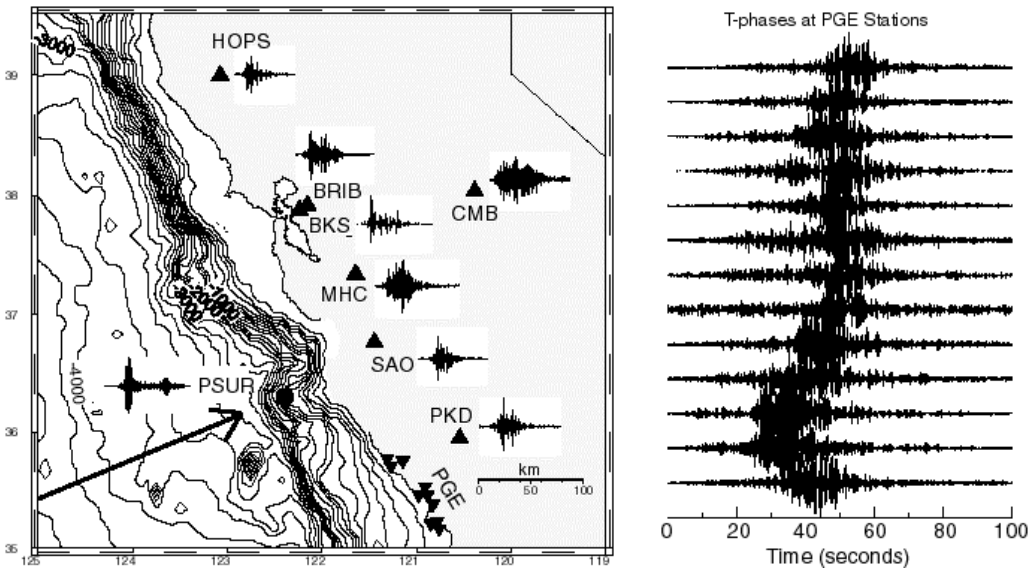

FIGURE 2. RECORDS FROM THE JUNE 30, 1997 LOIHI EVENT AND STATION LOCATIONS. THE PROPAGATION DIRECTION IS INDICATED BY THE ARROW, WHICH POINTS TO THE HYDROACOUSTIC STATION PSUR (INDICATED BY THE CIRCLE). 150 SECONDS OF THE T-PHASE RECORD IS SHOWN TO THE STATION'S LEFT. THE BDSN STATIONS (LARGE TRIANGLES) AND CORRESPONDING RECORDS ARE INCLUDED ON THE MAP ON THE SAME SCALE. THE PG&E STATION LOCATIONS ARE INDICATED BY INVERTED TRIANGLES AND THEIR WAVEFORMS ARE SHOWN TO THE RIGHT, IN ORDER OF INCREASING DISTANCE FROM BOTTOM TO TOP. THE ARRIVAL TIMES DO NOT CORRESPOND WELL TO TOTAL DISTANCE BECAUSE THE DISTANCE FROM THE CONVERSION POINT VARIES. THE BATHYMETRY IS CONTOURED IN 200 METER INTERVALS.

We calculated T-phase transfer functions for this data set by taking the ratio of the instrument corrected spectral amplitudes of the seismic stations to the Point Sur station for all good quality data at the PG&E stations and the 6 coastal BDSN stations (CMB was excluded because it is much farther inland). The spectral ratios were averaged for all events for each station. Two stations recorded all four events, 7 stations recorded 3, 9 stations recorded 2, and two stations recorded only 1 event. The resulting spectral ratios are shown in Figure 3. There is a clear decline in amplitude with frequency for both networks, but it is particularly pronounced for the BDSN network. This is likely due to greater attenuation of the higher frequencies because of the longer paths to the BDSN stations. Simulations discussed later in this paper indicate that much of the energy in the hydroacoustic wave is transmitted to land at approximately 200 m bathymetry, which corresponds to the contour line (Figure 2) nearest the coast. The crustal paths from the conversion point to the PG&E stations are only 5 to 20 km long, while paths to the BDSN stations are 40-75 km. Also shown in Figure 3 is an approximate upper bound on the transfer function derived from the simple case of a plane acoustic wave travelling in the ocean and propagating into a solid at normal incidence.

The ocean hydroacoustic phase may convert to a variety of complex phases due to the interaction with the coast. We can get some insight into the type of conversion that occurs by looking at far inland T-phases, and examining the propagation speeds of these waves. The T-phase from the 1997/06/30 event is large enough to be seen well inland from the California coast. Figure 4 shows two sets of seismograms recorded along the two (approximate) great circle paths. The paths are from SAO to KCC and from JRSC to MHC to CMB. Since the waveform is dispersed, there is some uncertainty about when to pick the arrival, however if we use the peaks of each wave train, then we get a velocity between SAO and KCC of 6.8 km/sec, and a velocity along the path of the other three stations of 5.6 km/sec. These velocities correspond to P-wave speeds, so the T-phases must be travelling as P-waves over this range.

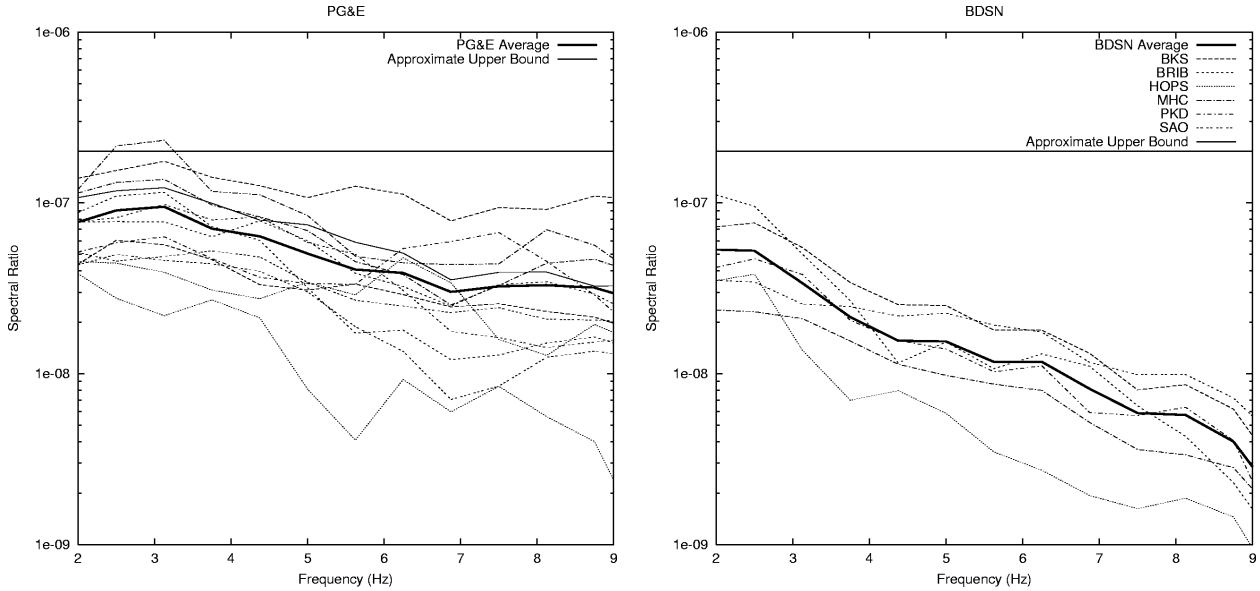

Figure 3. Ratios of seismic spectra at stations in California that recorded the Loihi events, divided by the Point Sur spectra. These are T-phase transfer functions converting pressure to vertical velocity. The frequency band shown here is from 2 to 9 Hz. The left plot shows PG&E stations and the right plot shows BDSN stations. The absolute amplitude of the PG&E records is uncertain, however the amplitude of the BDSN records, and the spectral shape of both sets of curves, are accurate. Also shown is the approximate upper bound for conversion from pressure in the ocean to particle velocity on land. The heavy line is the average log spectral ratio for all stations except far inland stations. Spectral ratios are in MKS units (meters/second/Pascal).

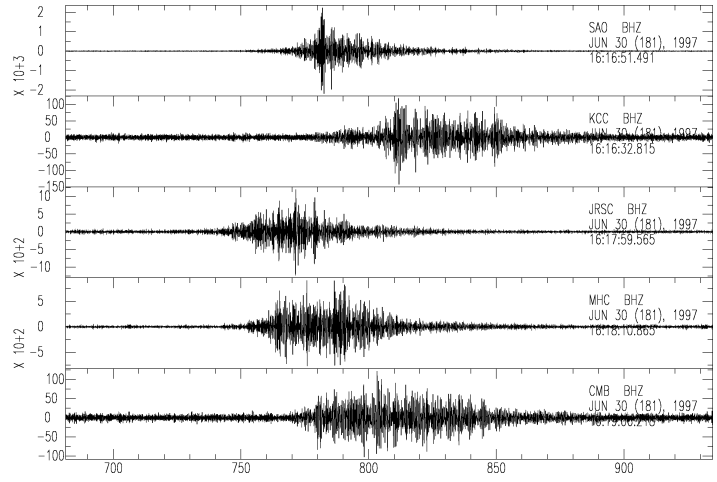

Figure 4. T-phases recorded near the coast and far inland from the 1997 June 30 Loihi event. The top two seismograms and the bottom three seismograms were recorded at stations along approximately the same great circle path. The horizontal axis is time in seconds. The data has been high pass filtered at 2 Hz.

Particle motion provides an independent means of assessing wave type. Figure 5 shows that the particle motion for the largest part of the record, near the front of the T-phase, is strongly linear. This part of the record is clearly dominated by body waves, most likely P-waves, in agreement with the conclusion from travel times. Linearity decreases later in the record, although it's not clear whether that is due to the arrival of later scattered P-wave energy, surface wave arrivals, or a mixture of phases. The particle motion of the earliest part of the T-phase is elliptical and retrograde, suggesting that this part of the wave train is composed of Rayleigh waves. This is consistent with the simulations later in this paper, which indicate that surface waves can precede the P-wave near the coast, due to earlier conversion of the T-phase in water to surface waves.

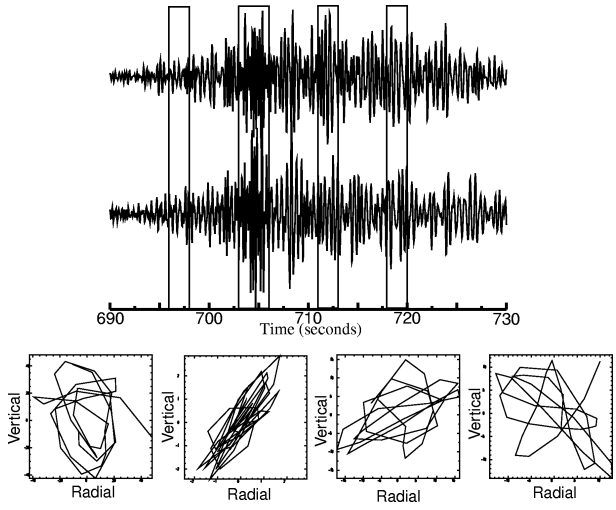

Figure 5. Vertical (top trace) and radial (lower trace) component seismograms from SAO for the 1997 June 30 event. Particle motions for four outlined time windows are shown below the seismograms. The very linear motion of the second time window indicates dominance there by body waves, and the elliptical motion of the first time window suggests that the early part of the wave train is composed of surface waves.

Two-dimensional finite difference calculation of propagation onto land

We use the two-dimensional finite difference code TRES2D to model the propagation of hydroacoustic waves onto the coast. TRES is a finite difference code developed at Maxwell Technologies (S-Cubed) with 2D and 3D versions that are used to model wave propagation. In this case we model a 2D slice of the propagation path. The normal mode code Kraken (Kraken can be obtained through the Ocean Acoustics Library web site at http://oalib.njit.edu/) was used to calculate the acoustic wave field in the ocean at a distance of 3710 km from Loihi. This solution was used as the source in the finite difference calculation using the representation theorem (see Stevens et al, 2000 for implementation details). Even though this is a two-dimensional problem, it requires a very large calculation because the distances of interest are large, about 100 km, the wave speed in the water is slow, and we are interested in frequencies higher than 1 Hz. We used recursive grid refinement (McLaughlin and Day, 1994), with the top 5 km portion (including ocean and the upper oceanic crust) covered with uniform grid cells of 16.75m x 16.75m and the remaining grid with cells of 67m x 67m. The calculation is accurate to 9 Hz throughout all the grids and the simulation time is 100 seconds. The time step is 0.005s for 67m spacing and 0.00125s for 16.75m spacing.

Velocities for the full grid were saved for each second of time in the calculation, and these were used to create images and animations of the velocity fields to help visualize the evolution of the velocity field. There is a gradual decay of the hydroacoustic wave as it travels upslope, with body waves emitted continuously with varying amplitudes into the earth below, and a surface wave that gradually forms along the ocean bottom. At sharper bathymetric gradients the transmission is increased, and when the hydroacoustic wave reaches an ocean depth of 200 meters, there is a burst of energy much larger than anywhere else along the path. Strong surface waves are generated on land from the edge of the ocean to the boundary of the calculation. Figure 6 shows a snapshot of the horizontal displacement field at 65 seconds. The figure shows the burst of energy at 200 meter depth. Color animations of this calculation can be viewed online at http://www.maxwell.com/products/geop/Movies/hydro.htm. The calculated T-phases have some very odd properties. As can be seen in Figure 6, a strong surface wave develops quite early and

can be seen on land at 65 seconds, which is the same time that the burst of body waves occurs. Consequently the surface wave appears in the wave train before, and simultaneous with, the body waves generated by the final decay of the hydroacoustic wave. The T-phase near the coast is therefore a mixture of seismic phases.

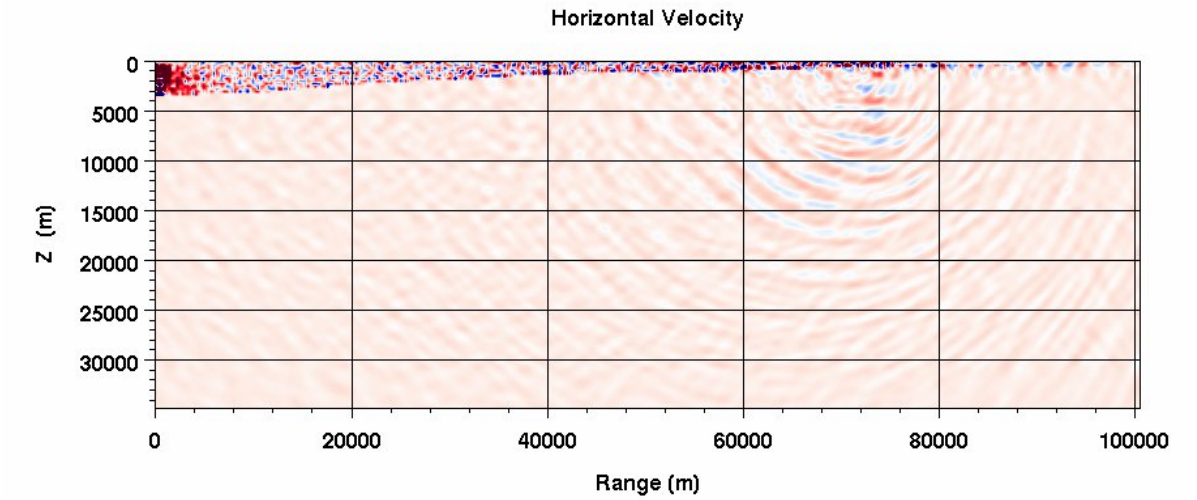

Figure 6. Snapshot of the calculation at 65 seconds. The dominant hydroacoustic arrival has reached a depth of 200 meters. At this point there is a burst of energy transferred as body waves from the ocean into land. Zero range corresponds to the point 3710 km from Loihi. The ocean/land interface at the surface is at location 87368.

The results of the calculation were saved with a much finer time resolution at selected locations along the surface, and at a depth of 740 meters in the center of the sound channel. Figure 7 shows the calculated horizontal velocity in the water at 47235 m, which corresponds approximately to the location of the Point Sur hydroacoustic station. Also shown are the horizontal and vertical components of the waveform on the surface at location 87904 m, which is on land close to the coast. The amplitude ratios between the velocity on land and in the water are about 0.2, which is consistent with our earlier estimates of the upper bound of the transfer function (note the earlier discussion was for pressure to velocity which adds a factor of about 10^{-7}). The waveforms on land are complex and longer in duration than the underwater waveform. From travel times and particle motion it is clear that the dominant energy is traveling at surface wave speeds. The complexity of the waveforms arises from the complex way the waves are generated over an extended region of the ocean bottom.

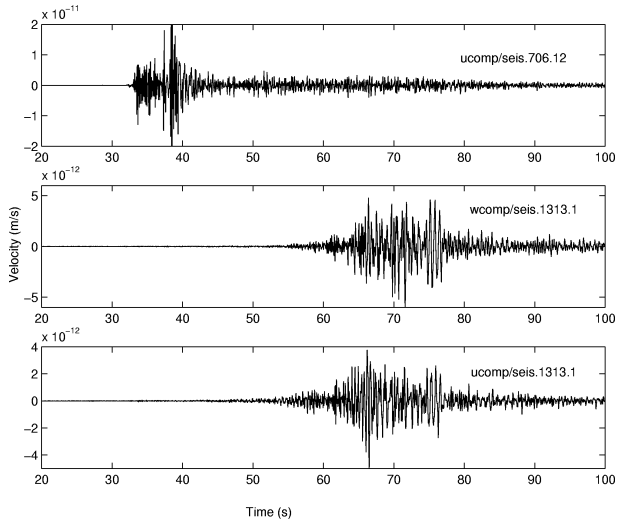

Figure 7. Calculated horizontal velocity at a depth of 740 meters in water at the location of the Point Sur station (top) and vertical (mid) and horizontal (bottom) components of the velocity on land close to the coast. The horizontal axis is time in seconds since the start of the calculation.

Figure 8 shows the spectral amplitude of the horizontal velocity in the 1-9 Hz frequency band underwater at the Point Sur location and the vertical velocity at a station on land close to the coast. The underwater spectrum is nearly flat across this frequency band. The spectra on land, however, exhibit a significant decline in amplitude with frequency, similar to the spectral decline observed for the coastal California stations. This suggests that during transmission from water to land, the higher frequencies scatter more strongly than the lower frequencies, leading to a decline in high frequency content in the coastal waveforms.

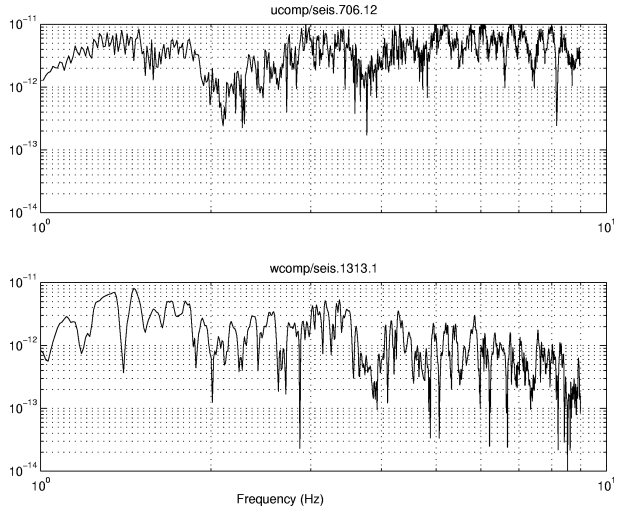

Figure 8. Calculated spectral amplitudes of the horizontal velocity at a depth of 740 meters underwater (top) and the vertical velocity at the surface on land near the coast (bottom).

We have used T-phase observations in water and on land together with numerical calculations of T-phase propagation from water to land in order to understand the nature of T-phase conversion. The results are complex and at first glance contradictory. Whereas T-phases are observed to travel at P-wave speeds on land, the calculations show strong surface waves near the coast. However, the calculations also show lower amplitude body wave arrivals even very close to the coast, and strong body waves propagated away from conversion points along the ocean bottom. Some of this body wave energy will return farther inland as P_g and P_n phases. The high frequency surface waves, on the other hand, can be expected to attenuate away very quickly and will not propagate to large distances. We therefore expect to see stronger surface waves than P-wave arrivals near the coast, with the surface waves dying out and the P-waves becoming dominant as the wave travels inland.

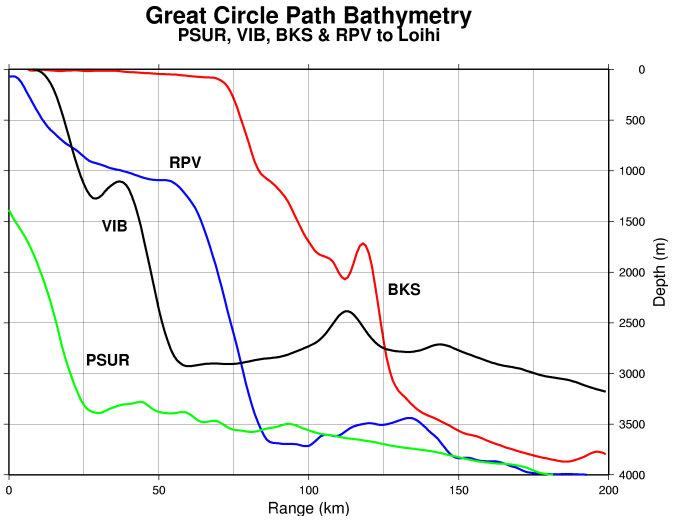

Figure 9. Great circle path showing bathymetry to PSUR, RPV, BKS, and VIB along the direction to Loihi from each station. Zero range corresponds to the station location. Vertical exaggeration makes the slopes appear steeper.

A similar study was performed by Piserchia et al (1998), in which they modeled T-phase conversion from an explosive source in the ocean, observed on the islands of Mururoa and Fangataufa in the South Pacific Ocean. They used ray tracing instead of a modal solution, and calculated Green's functions along a vertical boundary in order to propagate the source onto the islands. They found that the T-phase on land consisted of two P waves followed by two Rayleigh waves, where the multiple arrivals are identified as coming from different conversion points. The calculation was performed for a dominant frequency of 6 Hz, and in this case the calculated P and Rayleigh waves were found to be comparable in size. Cansi and Bethoux (1985) modeled far inland T-phases as converted T-P and T-S phases along a curve corresponding to a fixed depth in the ocean. They found good agreement with observed waveforms with synthetics composed only of P and S waves. Talandier and Okal (1998) studied conversion of T-phases on steep island slopes using data from the Polynesian Seismic Network and found from the observations and ray tracing arguments that the T-phase consisted primarily of P-waves at distances greater than 9 km from the conversion point. At closer distances, they found that the T-phase was more complex and composed primarily of S-waves and surface waves. They also suggested that only surface wave conversion would occur for slopes with angles of less than 16 degrees.

We have modeled propagation onto the California coast in considerable detail because of the availability of a good data set for comparison, and because we have stations both underwater and on land. The question arises as to how closely this models propagation onto the IMS T-phase stations which have different bathymetric profiles. Also, we would like to know how sensitive the calculations are to the details of the profile, and in particular to the slope of the ocean bottom on the approach to the coast. Figure 9 shows the bathymetric profiles off the coast of California in the direction of Loihi passing through the Point Sur, RPV, and BKS stations. Also shown for comparison is the profile in the direction of Loihi off the coast of VIB. Although they differ in detail, the structures are comparable in general features. The slope off the coast of VIB is similar to the slope off of BKS, although VIB is much closer to the coast. The slope through RPV is smaller. The slope used in the calculations is intermediate between these slopes. Note that there is considerable vertical exaggeration in these figures. Even the steepest part of the slope at VIB decreases by 1000 meters over a distance of 10 km, which corresponds to an angle of about 6 degrees. The steepest slopes off of the island T-phase stations change by 1000 meters over a distance of four km, an angle of about 14 degrees. To assess how much difference this caused, we ran three additional finite difference calculations, using the same ocean structure and modes as in the calculations above, but with constant slopes of 10, 20, and 30 degrees. In each case, the coastal boundary was fixed at 80 km from the left edge of the grid. The resulting vertical displacements at a point 7 km inland from the coast are shown in Figure 10. The waveforms are remarkably similar to each other and to the earlier calculations. The waveforms consist primarily of surface waves of comparable amplitude. The main difference is in the timing of the body wave which close examination shows arrives earlier than the surface wave for the 30 degree slope, and is within the surface wave wavetrain for the shallower slopes.

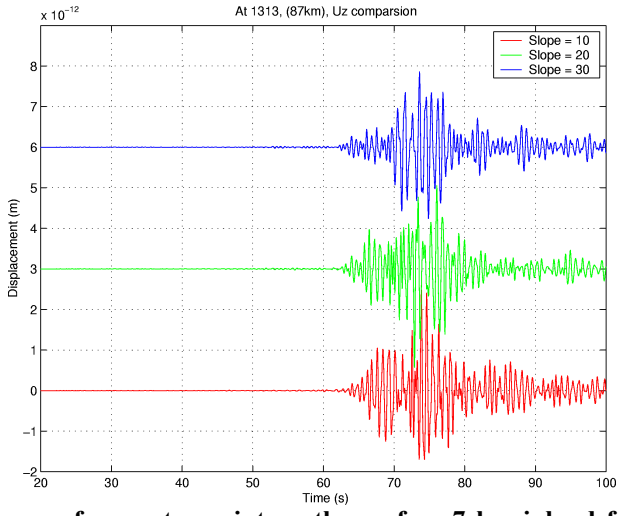

Figure 10. Vertical velocity waveforms at a point on the surface 7 km inland from the coast for the three calculations with slopes of 10 (bottom), 20 (middle), and 30 (top) degrees.

One of the conclusions that can be drawn from the calculations is that T-phases observed close to the conversion point should be dominated by surface waves. The calculations discussed above all had a low velocity layer near the surface, which could amplify the surface waves. To assess the magnitude of this effect, we performed another calculation with a uniform structure. The ocean was modeled as having a depth of 3500 meters and then a slope of 30 degrees up to the coast. Figure 11 shows the vertical component of velocity at a point 7 km from the coast for the two calculations with the uniform structure and the full structure including the low velocity layer. As expected, surface waves are smaller, however the wavetrain is still dominated by the surface waves which are much larger than the body waves at this distance. Body waves arrive at about 62 seconds. They are difficult to see, but can be identified by their particle motion.

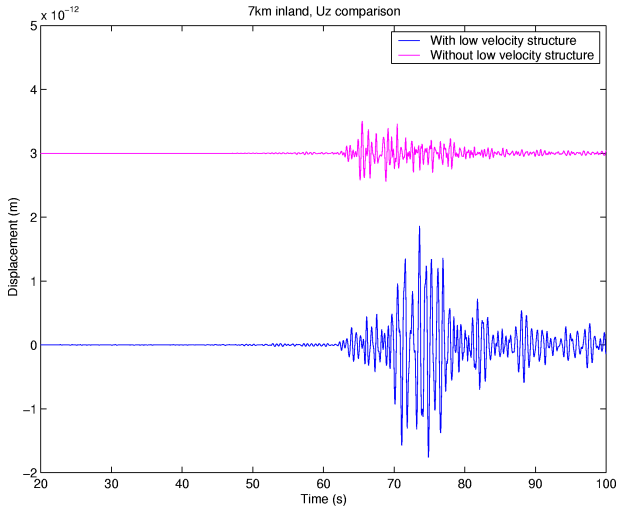

Figure 11. Vertical component of velocity on the free surface for calculations with a low velocity surface layer (bottom) and without (top).

Conclusions and Recommendations

We have used observations of T-phases underwater and on land to directly measure the transmission of energy from ocean to land, and have performed numerical simulations of T-phase propagation from ocean to land to obtain a better understanding of this process. The observations show that there is a significant decline in spectral amplitude with frequency on land compared to observations in the ocean. The observations also show that T-phases propagate primarily as P-waves once they are far enough inland. The numerical simulations provide considerable insight into the phenomena that occur when hydroacoustic waves propagate onto land. The calculations reproduce the spectral degradation observed in Coastal California stations. Both the calculations and the observations show that T-phases observed near the coast are composed primarily of surface waves. Because the surface waves are generated over a more extended region than body waves, they may arrive at near coastal stations earlier than the body wave and obscure any body wave arrivals.

Continuing research is needed to evaluate the response of the IMS T-phase stations. The calculations and parameter studies performed to date provide considerable insight into the expected response at these stations. The calculations cover the range of slopes offshore of the IMS stations, so we believe the effect of slope in general has been adequately modeled. However, specific calculations of T-phase conversion should be performed for each station along different angles of approach. Three dimensional calculations may be required to model the response of the island T-phase stations.

Acknowledgement
We thank Marcia McLaren of Pacific Gas and Electric for the use of her data and for pointing out to us the large T-phases from the Loihi events.

Key Words: hydroacoustic, T-phase, finite difference, IMS

References

Achenbach (1973), Wave Propagation in Elastic Solids, North-Holland Publishing Company, New York. Cansi, Y. and N. Bethoux (1985), "T waves with long inland paths: synthetic seismograms," J. Geophys. Res., V. 90, pp. 5459-5465.

D'Spain, G. L., L. P. Berger, W. A. Kuperman, J. L. Stevens, and G. E. Baker (1999), "Normal mode composition of earthquake T-phases," submitted to Pure and Appl. Geophys.

Eneva, M., J. L. Stevens, J. R. Murphy, and B. D. Khristoforov (2000b), "Effect of charge depth in Russian hydroacoustic data from nuclear and HE explosions," Proceedings of the 22nd Annual DOD/DOE Seismic Research Symposium, 12-15 September, 2000.

Eneva, M., J. L. Stevens, B. D. Khristoforov, J. R. Murphy, and V. V. Adushkin (2000a), "Analysis of Russian Hydroacoustic Data for CTBT Verification", Pure and Applied Geophysics, in press.

Eneva, M., J. L. Stevens, J. Murphy, B. D. Khristoforov and V. V. Adushkin (1999), "Analysis of Russian Hydroacoustic Data for CTBT Verification", Proceedings of the 21st Seismic Research Symposium on Monitoring a Comprehensive Test Ban Treaty, 21-24 September, 1999.

McLaughlin, K. L. and S. M. Day (1994). "3D Elastic Finite-Difference Seismic-Wave Simulations, Computers in Physics," 8, #6, pp 656-663.

Piserchia, P. F., J. Virieux, D. Rodrigues, S. Gaffet and J. Talandier (1998), "Hybrid numerical modelling of T-wave propagation: application to the Midplate experiment," Geophys. J. Int., V. 133, pp 789-800.

Stevens, Jeffry L., G. Eli Baker, Ron W. Cook, Gerald D'Spain, Lewis P. Berger, and Steven M. Day (2000), "Empirical and Numerical Modeling of T-Phase Propagation from Ocean to Land", Pure and Applied Geophysics, in press.

Stevens, Jeffry L., G. Eli Baker, Ron W. Cook, Gerald D'Spain, Lewis P. Berger, and Steven M. Day (1999), "Empirical and Numerical Modeling of T-Phase Propagation From Ocean to Land", Proceedings of the 21st Seismic Research Symposium on Monitoring a Comprehensive Test Ban Treaty, 21-24 September, 1999.

Stevens, J. L., G. E. Baker, J. R. Murphy, R. W. Cook, G. D'Spain, L. P. Berger, and B. D. Khristoforov (1998), "T-Phase Excitation and Transfer Function Research," Proceedings of the 20th Seismic Research Symposium on Monitoring a Comprehensive Test Ban Treaty, 21-23 September.

Talandier, J. and E. A. Okal (1998), "On the mechanism of conversion of seismic waves to and from T waves in the vicinity of island shores," Bull. Seism. Soc. Am., V.88, pp. 621-632.